Roman CCS White Paper
The Demographics of Transiting Exoplanets across all Major Milky Way Environments

Robert F. Wilson[1], Thomas Barclay[1], Jesse Christiansen[2], Néstor Espinoza[3,4], B. Scott Gaudi[5], Christina Hedges[1], Veselin B. Kostov[1,6], Susan Mullally[3], Elisa Quintana[1], Joshua Schlieder[1], and Allison Youngblood[1]

[1]NASA Goddard Space Flight Center, Greenbelt, MD, 20771, USA
[2]Caltech/IPAC-NASA Exoplanet Science Institute, Pasadena, CA 91125, USA
[3]Space Telescope Science Institute, Baltimore, MD 21218, USA
[4]Department of Physics & Astronomy, Johns Hopkins University, Baltimore, MD 21218, USA
[5]Department of Astronomy, The Ohio State University, Columbus, OH 43210, USA
[6]SETI Institute, Mountain View, CA 94043, USA

Roman Core Community Survey: Galactic Bulge Time Domain Survey

Scientific Categories: Exoplanets and exoplanet formation; Stellar populations and the interstellar medium

Additional Scientific Keywords: Transits, Planet Hosting Stars, Galactic Center

Submitting Author: Robert F. Wilson; robert.f.wilson@nasa.gov

Abstract

The Galactic Bulge Time Domain Survey (GBTDS) will survey $\gtrsim 10^8$ stars at an approximately 15-minute cadence with the expected photometric precision sufficient to detect >100,000 planets via transit (Wilson et al., 2023). The high stellar densities of the Galactic bulge fields, combined with the near-IR (0.93-2.00 μm) $F146$ bandpass will facilitate the detection of thousands to tens of thousands of transiting exoplanets in each of the Milky Way thin disk, thick disk, and bulge populations. Due to the chemical heterogeneity of these Galactic environments, comparing the occurrence of transiting planets within each sub-population will place significant constraints on planet formation theories such as core accretion, migration, and for small planets, even interior compositions. While the nominal design will be effective overall, we argue in this white paper that the proposed study can be optimized by prioritizing the search over a wider breadth of Galactic environments. More specifically, minimizing the observing cadence and controlling for low-amplitude correlated noise could nearly double the yield of small ($R_p \approx 2R_\oplus$) distant ($d \approx$ 2-3 kpc) exoplanets, and observing fields with a larger range of Galactic latitude will significantly increase the sampling of giant ($R_p > 8R_\oplus$) planets in the Fe-poor, α-rich thick disk population, providing significant constraints on planet formation that are not currently feasible with existing observatories.

1 Introduction and Scientific Motivation

The GBTDS will amass precise ($\sigma \sim$ 0.1-1% per exposure) time-series photometry on a staggering 40–60 million stars brighter than $F146 \sim 21$ (Penny et al., 2019; Wilson et al., 2023). Extrapolating from Kepler occurrence rates, these stars will yield between 60,000 and 200,000 transiting planets, depending on the exact relationship between stellar composition and planet occurrence (Montet et al., 2017; Wilson et al., 2023), and even more transiting planets will be detectable as dim as $F146 \approx 22$. This yield will be comprised primarily of giants ($R_p > 4R_\oplus$) with close-in orbits ($a < 0.3$ au), although between 7,000 and 12,000 small planets ($R_p < 4R_\oplus$) should also be detectable. The power in this paradigm-shifting survey will be two-fold: first, in the depth and breadth of the stellar populations that will be surveyed (see Figure 1), and second, in the statistical power represented by the order of magnitude increase in the number of known exoplanets, all of which will be uniformly observed and detected.

1.1 Stellar Composition as a Probe of the Planet-forming Environment: Population Constraints on Core Accretion, Migration, and Interior Compositions

Planet occurrence, particularly for giant planets ($R_p \gtrsim 4R_\oplus$, $M_p \gtrsim 30M_\oplus$), is known to be intimately correlated with stellar metallicity (Fischer & Valenti, 2005; Johnson et al., 2010; Ghezzi et al., 2010; Wang & Fischer, 2015; Petigura et al., 2018; Wilson et al., 2022). This correlation is typically interpreted in the context of the core accretion planet formation model. In this scenario, an increased stellar metallicity is assumed to correlate with higher solid surface densities in the protoplanetary disk which facilitate the rapid growth of planetary cores up to a threshold mass of $\sim$10 $M_\oplus$, at which point the planetary cores will accrete a gaseous envelope (Pollack et al., 1996; Ida & Lin, 2004; Mordasini et al., 2012; Chabrier et al., 2014). However, the growth of planetary cores may be sensitive to enhancements in specific elements. For example, silicates may be needed to seed planetary cores (Natta et al., 2007), and CNO ices constitute a significant fraction of the mass in planetesimals beyond the water ice line (Pontoppidan et al., 2014) where core accretion is most efficient (see, e.g., Dawson & Johnson, 2018, and references therein). Therefore, it is theoretically motivated that core accretion can be more effectively facilitated by the enhancement of specific α elements (elements with even atomic numbers, primarily generated in core-collapse supernovae; e.g., C, O, Mg, Si) rather than just bulk metallicity. Thus, the GBTDS data will yield a critical test of core accretion by measuring the relative occurrence of giant planets in Fe-poor, α-rich environments (e.g., thick disk, bulge) and Fe-rich, α-poor environments (e.g., thin disk).

The period distribution of giant planets in each Galactic environment will place significant constraints on the efficiency of giant planet migration. The GBTDS should detect $\sim$1000s of cool ($a \sim$ 1-3 au), single-transiting giant planets near the water ice line, where recent studies of RV-detected exoplanets have shown an abundance of giant planets (Fernandes et al., 2019; Fulton et al., 2021). Measuring the relative occurrence of cool Jupiters and hot Jupiters, particularly as a function of stellar composition, will clarify the migration mechanism for hot Jupiters. For instance, because there is evidence that planet-planet dynamical interactions are more common in metal-rich host stars (Dawson & Murray-Clay, 2013), an increase in the occurrence of hot Jupiters relative to cool Jupiters for such host stars would indicate that planet-planet dynamical interactions are a significant migration pathway for hot Jupiters.

The composition of the stellar host is also hypothesized to correlate with the internal structure of small planets. Simulations show that variations in host star [Fe/H] and [α/Fe] can

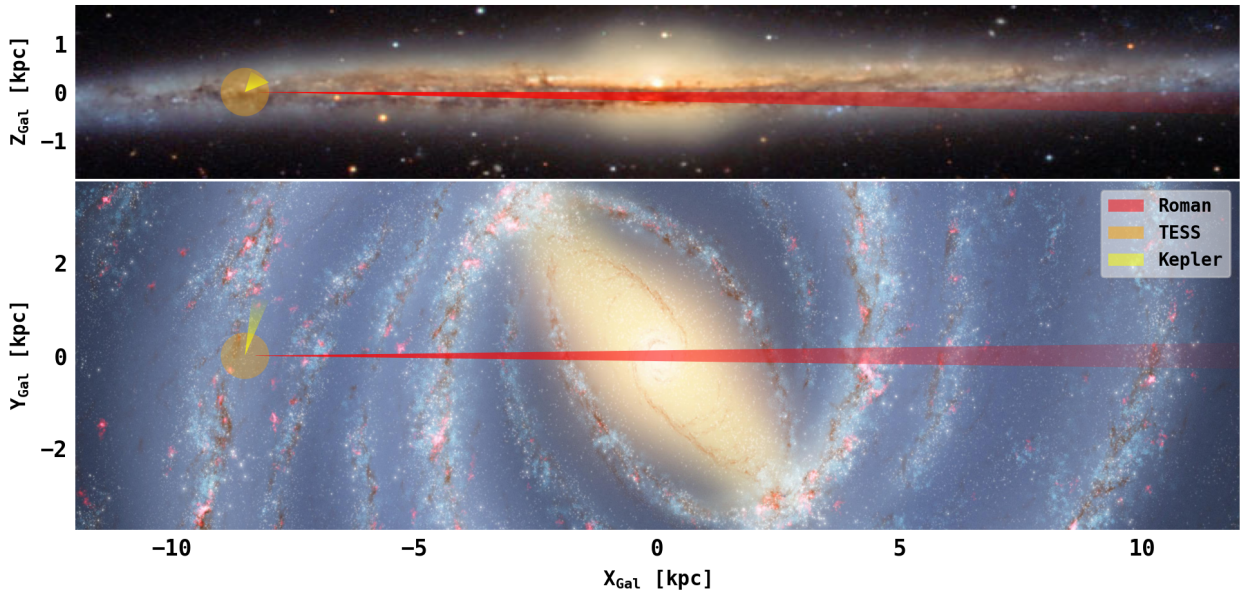

Figure 1: Roman will find exoplanets across all major components of the Milky Way outside the local stellar neighborhood. The shaded regions denote the maximum Galactic reach of Roman (red), TESS (orange), and Kepler (yellow). The artist's representations in each panel highlight the diversity of populations surveyed. **Top:** The reach of transit surveys outside of the Galactic midplane. **Bottom:** The reach of transit surveys within the Galactic midplane, highlighting the broad Galactic radii probed by Roman. Top image credit: J. Skowron / OGLE / Astronomical Observatory, University of Warsaw. Bottom image credit: NASA/JPL-Caltech.

lead to planets with different bulk compositions, for instance dividing into water-rich worlds and iron-rich, rocky worlds (Cabral et al., 2019). Indeed, recent observational results indicate that the small planet radius valley (Fulton et al., 2017) might be more correctly characterized as a small planet density valley, at least for M dwarf planet hosts, separating planets with distinct bulk compositions: rocky worlds, water worlds, and puffy mini-Neptunes (Luque & Pallé, 2022). If all of the above is true, then Roman should find that the relative occurrence of small planets, particularly from $R_p \approx$ 1.5-2.5 $R_\oplus$ which seem to consist of primarily water worlds, varies with Galactic environment, decreasing in the metal-rich thin disk, which should instead be dominated by rocky worlds primarily with radii $R_p \lesssim 1.5 R_\oplus$, assuming a similar mass distribution. In essence, a dearth of small planets with M dwarf hosts at $R_p \approx$ 1.5-2.0 $R_\oplus$ should be more prominent in metal-rich environments, provided that interior compositions are indeed correlated with stellar abundances.

1.2 Roman Transiting Planets are Essential for a Robust $\eta_\oplus$ Microlensing Estimate

The Kepler mission (Borucki et al., 2010) was unable to fully achieve its primary goal of deriving $\eta_\oplus$—the frequency of Earth-sized planets in the habitable zones of Sun-like stars. Unexpectedly high stellar noise and hardware failures resulted in too few high-quality planet candidates in the relevant parameter space for robust occurrence rate calculations. Thus, the current state-of-the-art estimates range from $\eta_\oplus \approx$ 5–30% (see, e.g. Kunimoto & Matthews, 2020; Bryson et al.,

2021; Bergsten et al., 2022). Tighter constraints on $\eta_\oplus$ have direct implications for the design of future missions, including NASA's next flagship mission, the Habitable Worlds Observatory. One upcoming chance – and possibly the only upcoming chance – to improve our understanding of $\eta_\oplus$ is the Roman microlensing survey, which will be sensitive to Earth-mass planets in the habitable zones of Sun-like stars (Penny et al., 2019).

However, there is a large confounding variable in the microlensing planet-search population, which will differ significantly in Galactic environment from the local stellar neighborhood probed by Kepler. Therefore, there is a significant risk that combining two incompatible datasets could further erode our understanding of $\eta_\oplus$. However, the Roman *transit* survey will probe the distant, short period planet population, which can then be directly compared with the equivalent local population from Kepler. By constraining the impact of Galactic location on the small planet population, the Roman transit survey will anchor the interpolation across host mass and planet period that is necessary to reliably combine the Roman microlensing and Kepler transit surveys and provide a robust, joint estimate of $\eta_\oplus$.

2 Optimizing the GBTDS for Distant Exoplanet Demographics

2.1 Expected Results for the Nominal GBTDS design

Wilson et al. (2023) combined a custom Galactic population model and planet occurrence rates measured from the Kepler survey with pixel-level simulations of Roman Wide Field Imager to estimate the expected transiting planet yield for bright stars ($F146 < 21$) in the nominal GBTDS design. This design consisted of six 72-day seasons, clustered at the autumnal and vernal equinoxes, with each sector consisting of seven fields, and the time between the start of successive sectors (i.e., sector duration/cadence) of 15 minutes, and an effective exposure time of 54 seconds. Under these parameters, the GBTDS should yield ∼60,000-200,000 transiting planets, including ∼1,000s of gas giants with distances >12 kpc and ∼1,000 planets with $R_p < 2R_\oplus$ at distances of ∼1-3 kpc. Because these results only apply to bright stars ($F146 < 21$), this is a conservative estimate, particularly for close-in giant planets which have a high detection efficiency ($p_{\rm det} \approx 90\%$) for G-type dwarfs at $F146 = 21$.

Assuming that the number of pixels used to extract photometry remains constant for stars with $F146 > 21$, photon noise from crowding will dominate the error budget for dim stars. Under these assumptions, hot Jupiters ($P < 10$ days) should still be detectable at distances of $d \gtrsim 25$ kpc, consistent with a G5V star at $F146 \approx 22$ mag, while the detectability of Saturn-sized planets ($R_p \approx 9R_\oplus$) at similar orbital periods will begin to diminish. For small planets with $R_p \approx 2R_\oplus$ and $P \approx 10$ days, the GBTDS will be sensitive to detecting transits from K- and M-type host stars at distances of $d \lesssim 3$ kpc. The stellar population at these maximum distances in the GBTDS should be dominated by old, thin disk stars with an average metallicity of [Fe/H] ≈ 0.18 dex (Anders et al., 2014; Eilers et al., 2022), resulting in a stellar population that is chemically distinct from the local stellar neighborhood.

Thus, along a particular line of sight, our ability to constrain the occurrence of close-in, giant planets as a function of Galactic environment should be limited only by the heterogeneity of the Milky Way itself. However, GBTDS design choices will significantly impact the detectability of small ($R_p \approx 2R_\oplus$) transiting planets.

2.2 Optimization Goals

Because the chemical abundance distributions of stars in the Galaxy vary significantly with $R_{\rm Gal}$, the Galactocentric radius, and $Z_{\rm Gal}$, the height above (or below) the Galactic midplane (Hayden et al., 2015; Eilers et al., 2022), our science goals can best be accomplished with a strategy that optimizes the range of $R_{\rm Gal}$ and $Z_{\rm Gal}$ searched for planets, which we use as a proxy for the average stellar composition (i.e., the [α/Fe] and [Fe/H] distributions).

A wider range of $R_{\rm Gal}$ can be probed by increasing the maximum distance at which transiting planets are detectable. Thus, one of our primary motivations is to increase the transiting planet detection efficiency (i.e., the probability that an arbitrary transiting planet is detected; $p_{\rm det}$) at large distances which can be modeled by a single parameter, the expected transit signal-to-noise ratio ($S/N_{\rm exp}$). This quantity can be approximated by

$$S/N_{\rm exp} = \frac{R_p^2/R_\star^2}{\sigma_{\rm dpp}\sqrt{t_{\rm sector}/t_{\rm dur}}}\sqrt{n_{\rm s}T_{\rm s}/P} \quad , \tag{1}$$

where R_p is the planet radius, $R_\star$ is the stellar host radius, n_s is the number of seasons, T_s is the season duration, P is the orbital period, $t_{\rm sector}$ is the sector duration (equivalent to the observing cadence), $t_{\rm dur}$ is the transit duration derived assuming a circular orbit, and $\sigma_{\rm dpp}$ is the single exposure differential photometric precision. Of these parameters, only n_s, T_s, and $t_{\rm sector}$ are directly dictated by the survey strategy. While $\sigma_{\rm dpp}$ may be optimized by increasing or decreasing the effective exposure time, such changes will inevitably lead to changes in $t_{\rm sector}$. Thus, most of our discussion for optimizing $S/N_{\rm exp}$ will focus on reducing $t_{\rm sector}$.

The opposite strategy from what is advocated here would be to instead optimize the survey for bright stars, and increase the surveyed area (or number of fields) at the expense of a longer $t_{\rm sec}$. This has several advantages as well, including a lower false positive rate, fewer candidates with blended transit depths, and transiting planets that can be more accurately characterized. However, considering the large number of transiting planets already expected in the bulge and nearside of the disk, surveying larger distances should provide more leverage in understanding the role of the Galactic environment. With regard to the treatment of false positives caused by eclipsing binaries, the strategy proposed in this paper would instead increase the light curve quality of dim stars, facilitating the assessment of quantities such as the background eclipsing binary rate, which can be used to model planet demographics at the catalog level jointly with the false positive rate, as advocated in Wilson et al. (2023). Thus, while any one planet candidate at large distance may be unreliable, the catalog itself, modeled jointly with the eclipsing binary rate, should still be incredibly powerful.

2.3 Sector Duration and Surveyed Area

The sector duration (i.e., the cadence) is set by the sum of the exposure time per field, the number of fields (i.e., the surveyed area), and the time needed to slew between fields. Generally speaking, increasing the surveyed area will increase the yield of nearby transiting planets and reducing the sector duration will increase the yield of distant transiting planets and small transiting planets. For small transiting planet candidates with bright host stars, these trade-offs are nearly equal and the total overall transiting planet yield is generally stable to within a few percent. However, due to our goals of detecting as many distant planets as possible, we advocate for reducing the sector duration as much as is feasible.

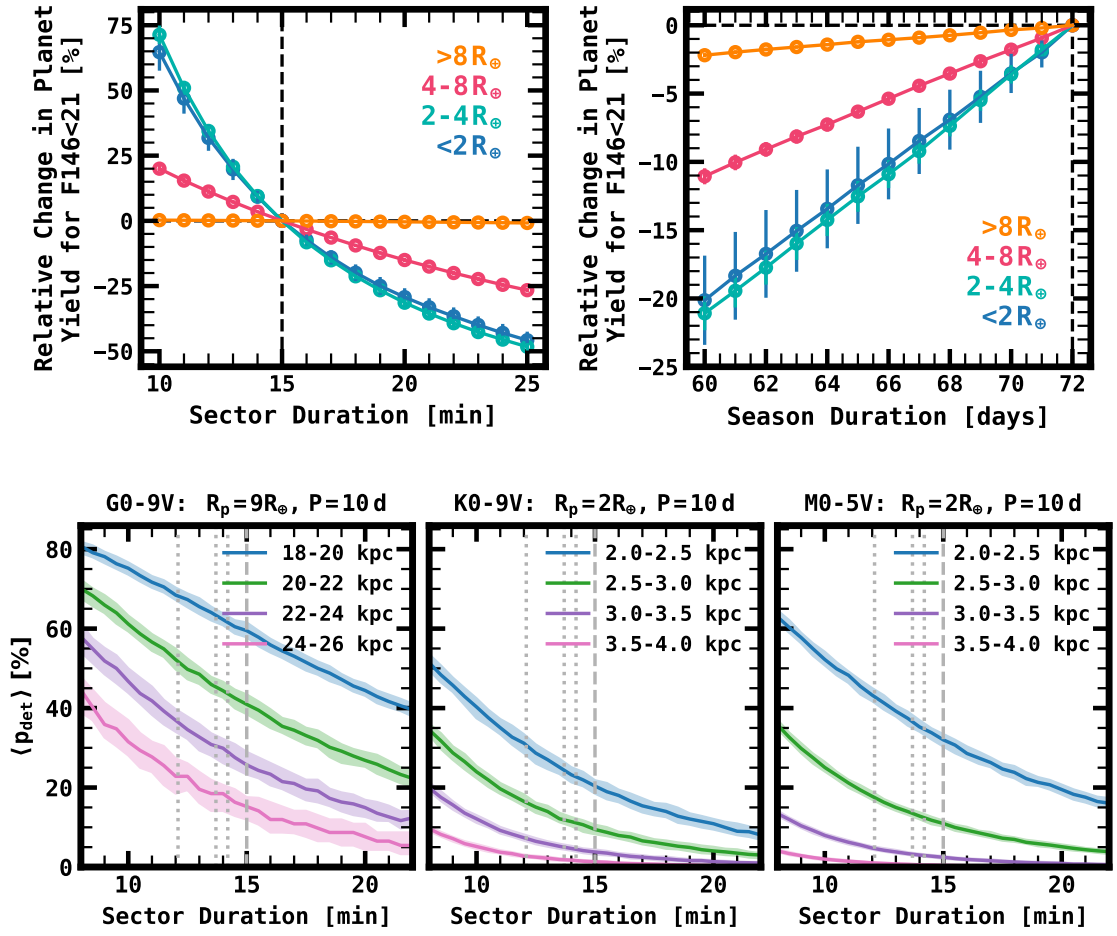

Figure 2: Top Row: The change in planet yield for bright sources ($F146 < 21$) per field relative to the nominal design as a function of planet size for variations in sector duration (left) and season duration (right). Each color represents planets of different sizes, Jupiters: orange, sub-Saturns: pink, mini-Neptunes: teal, and super-Earths: blue. **Bottom Row:** The average detection efficiency, $\langle p_{\rm det} \rangle$ over the range of stellar spectral types, for various distances as a function of sector duration for a hot gas giant with a G-dwarf host (left), a super-Earth with a K dwarf host (middle), and a super-Earth with an early M dwarf host (right). The gray lines show the sector duration of the nominal GBTDS design (dashed) and sector durations for the field layouts described in Section 2.5 (dotted).

To illustrate the trade between sector duration and number of fields surveyed, we calculate the probability that a transiting planet with $R_p = 2R_\oplus$, $P = 10$ days, will be detected ($p_{\rm det}$) using the detection efficiency model from Wilson et al. (2023). The results for K-type dwarfs and for early M-type dwarfs are shown in the bottom row of Figure 2. In the parameter space of interest, $d \approx$ 2-3 kpc and $R_p \approx 2R_\oplus$, a reduced sector duration from 14 to 12 minutes results in a 50-70% increase in $p_{\rm det}$ for K-type stars, and a 40-70% increase in $p_{\rm det}$ for M-type stars. Thus, reducing the number of fields from seven to six will result in reducing the sector duration by approximately 2 minutes (1 minute exposure + 1 minute slew/settle time), which will more than offset the $\sim$14% reduction in the total number of stars surveyed, particularly at larger distances. Similar advantages can be seen in the detectability of short-period ($P \approx 10$ days) Saturn-sized ($R_p \approx 9R_\oplus$) planets with G dwarf hosts at distances of $d \gtrsim 20$ kpc. For these reasons, we advocate for reducing sector duration, even at the expense of reducing the number of fields from seven (or eight) to six, provided that the microlensing goals can still be accomplished.

2.4 Season Duration

The duration of the GBTDS observing seasons is constrained on the short end by the requirement to resolve microlensing events with timescales of $2t_E \approx 60$ days (Gaudi, 2012), and on the long end by the visibility window of the bulge fields, which last for a maximum of 72 days. A reduction in season duration from 72 days to 60 days results in a $\sim$20% reduction in the yields of low-S/N transiting planets, decreasing approximately linearly by just under 2% per day lost from the season duration (see Figure 2, top right). For this reason, we advocate for as long a season duration as is feasible.

2.5 Field Locations

For the goals of this white paper, the location of the final GBTDS fields have two primary concerns. First, all fields should be adjacent to reduce the number of large slews so that sector durations can be minimized. As shown, an additional 2 minutes added to the sector duration can significantly undermine the goal of studying the demographics of distant ($d \approx 3$ kpc) small planets. Thus, we advocate against the addition of extra GBTDS fields, particularly if they are not adjacent to the primary fields.

Second, a larger range in Galactic latitude will result in more effective demographics of giant planets in the α-rich, metal-poor thick disk population, providing considerable leverage in disentangling the degeneracy between planet occurrence and [α/Fe] against [Fe/H]. This would increase the sampling of $Z_{\rm Gal}$, over which the relative density of thin and thick disk stars changes rapidly, particularly at $R_{\rm Gal} \approx$ 3-7 kpc on the far side of the bulge ($d \approx$ 12-16 kpc). Due to the relative scale heights and densities of the thin and thick disk ($h_{\rm Z,thin} \approx$ 150-350 pc, $h_{\rm Z,thick} \approx$ 500-1000 pc), the thick disk begins to dominate the stellar population at $Z_{\rm Gal} \gtrsim 500$ pc (Sanders & Binney, 2015; Li & Zhao, 2017; Li et al., 2018). However, due to the radial scale length of the thick disk, $h_R \approx$ 2-3 kpc, surveying a similar range of $Z_{\rm Gal}$ at $R_{\rm Gal} > 7$ kpc will have diminishing returns. To illustrate this point, we present two designs that can accomplish this goal by including a field centered at $b = -2.4°$ (referred to hereafter as D1 and D2; see Figure 3). The D1 and D2 designs will survey stars with maximum $Z_{\rm Gal} \approx$ 590-790 pc at distances of $d \approx$ 12-16 kpc. For comparison, the fields in the nominal design are only sensitive to $Z_{\rm Gal} \approx$ 420-560 pc at distances of $d \approx$ 12-16 kpc.

D1 and D2 illustrate the trades between adding an additional field and moving existing fields from the nominal design. For each field design we calculated $t_{\rm sector}$ using the expected slew/settle

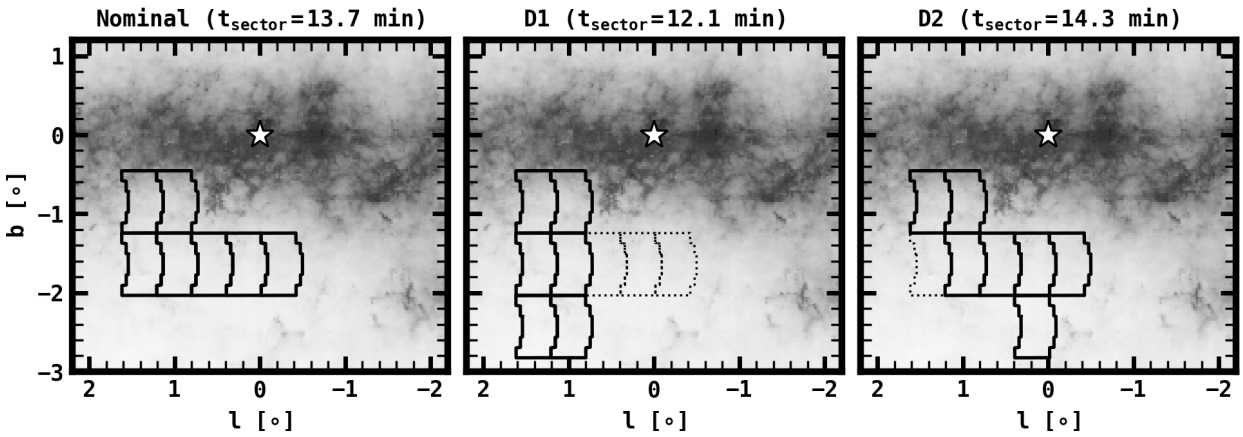

Figure 3: The nominal GBTDS field locations from Penny et al. (2019), compared with two additional field designs, D1 and D2, discussed in Section 2.5. The star is the location of the Galctic center, and the shading shows the extinction in the Galactic Bulge fields, converted from the reddening map determined by Surot et al. (2020). Due to the addition of diagonal slews and longer slews, moving a single field for design D2 inflates $t_{\rm sector}$. D1 minimizes $t_{\rm sector}$ by eliminating diagonal slews and removing one field, but neglects the fields at $l \approx 0°$ with the highest microlensing event rates.

times for Roman assuming six reaction wheels. To find the permutation that minimized $t_{\rm sector}$, we solved a variant of the traveling salesman problem. In determining a reasonable design, we optimized D1 purely for the proposed science investigation. That is, we reduced the number of fields to six to minimize $t_{\rm sector}$, and evenly sampled the Galactic latitude from $-0.4° < b < -2.8°$. The Galactic longitude for the D1 fields was chosen to minimize long slews and diagonal slews, which are the primary culprits in unnecessarily inflating $t_{\rm sector}$. D2, on the other hand, was chosen to preserve the fields near $l \approx 0°$, where the microlensing event rates are highest (Penny et al., 2019). However, as a result, $t_{\rm sector}$ is inflated by ∼30 seconds from the nominal design, despite having the same number of fields.

2.6 Correlated Instrumental Noise and other Low-Amplitude Systematics

The ability for Roman to detect small transit depths relies on increasing the transit S/N over many events. For white noise, the transit signal-to-noise is proportional to $\sqrt{n_p}$, where n_p is the number of data points collected in transit. In the presence of significant correlated noise, particularly on timescales of 2-3× a typical transit duration ($\lesssim$12 hours), the signal-to-noise increases more slowly, jeopardizing the ability to detect small planets. The dominant source of such systematics is difficult to predict at this time, but it may arise from a number of effects including detector non-linearities, persistence, and intra-pixel sensitivity variations.

To place requirements on the magnitude of correlated noise that can be tolerated by our science goals, we assume that the amplitude of correlated noise corresponds to a strict, minimum detectable transit depth for all exoplanets. Under these assumptions, Wilson et al. (2023) calculated the decrease in planet yields for bright stars under correlated noise levels ranging from 1.5 ppt to 0.1 ppt. These losses are shown in Table 1. Based on these results, we advocate for a goal of reducing correlated systematic noise to <0.5 ppt, which should ensure that the

	Amplitude of Systematics (ppt)				
$R_p/R_\oplus$	1.5	1.0	0.5	0.3	0.1
$\leq$2	36%	23%	8.2%	4.3%	<1%
2-4	31%	16%	2.8%	<1%	<1%
4-8	12%	5.7%	1.1%	<1%	<1%
>8	1.3%	<1%	<1%	<1%	<1%
All	7.0%	3.6%	<1%	<1%	<1%

Table 1: The decrease in the expected transiting planet yield under the assumption that correlated instrumental noise places a constraint on the minimum detectable transit depth. If correlated systematics can be controlled to <0.3 ppt, the planet yield will be unaffected.

yield of small planets would decrease by <10%, with a stretch goal of <0.3 ppt.

2.7 Dithering Strategy

Unlike previous transit surveys which placed a strict emphasis on pointing stability to reduce systematics for differential aperture photometry, the GBTDS observations will be dithered to enable astrometry for a myriad of other science goals. Because optimizing photometric surveys for transit detection requires precise but not necessarily accurate photometry, dithering is often discouraged as it can introduce instrumental systematics, e.g., from intra- and inter-pixel sensitivity variations. Therefore, we advocate for a dithering strategy in which such systematics can be precisely corrected. We argue for pixel-level, and sub-pixel dithers, essentially keeping the position of the star constant within 1-2 pixels. That way, algorithms to correct for such systematics (e.g., pixel-level decorrelation; Deming et al., 2015), can be more effective. In addition, persistence effects should be relatively stable, as stars from previous exposures will be illuminating the same set of pixels in each exposure. This will allow for a more precise treatment of persistence, as the magnitude of such effects is known to vary with detector location.

Dithering has an additional benefit for transit surveys, in improving the effectiveness with which false positives caused by blended eclipsing binaries can be identified. Such false positives can often be detected via difference imaging, where images during a transit are subtracted from images collected just before and after the transit. Performing astrometry on the residual image will then reveal the location of the transit signal. If discrepant with the location of the assumed source of transit, then the signal is rejected as a false positive. Dithered observations, which improve the PSF sampling, would allow this measurement to made more precisely. For this reason, the dithering strategy should be adequate to fully sample the PSF on typical transit duration timescales of $\lesssim$3-6 hours.

3 Summary

In this white paper, we motivate the goals of detecting transiting planets in the GBTDS across all major Galactic environments. The demographics studies performed from this catalog will place significant constraints on planet formation and migration. Optimizing the GBTDS for these science goals primarily relies on improving the detection efficiency of small planets at distances of $d \approx$ 2-3 kpc. For giant planets, the GBTDS can be optimized by increasing the diversity of surveyed stellar populations, particularly in the thick disk. In assessing these goals we provide recommendations to the GBTDS survey strategy, which are reiterated below.

- The sector duration ($t_{\rm sec}$; equivalent to the observing cadence) should be reduced at all costs. Reducing $t_{\rm sec}$ by two minutes can increase the detection rate of small, distant exoplanets by as much as 70%. Reducing the number of GBTDS fields from seven to six would be effective in this goal.

- The season duration should be as long as possible. For each day the season duration is decreased, the yield of small planets decreases by 2%.
- Placing one or two fields at $b = -2.4°$ will significantly increase the sampling of giant planets in the α-rich, Fe-poor thick disk.
- The amplitude of systematic correlated noise on timescales of $\lesssim$12 hours should be <0.5 ppt, with a stretch goal of <0.3 ppt. This ensures that the small planet ($R_p < 2R_\oplus$) yield will decrease by $\lesssim$10%.
- The dithering strategy should consist of small (pixel/sub-pixel) dithers to allow for consistent, precise systematics removal. The dither pattern should allow full sampling of the PSF on timescales of $\lesssim$3-6 hours to optimize relative astrometry for identifying blended eclipsing binaries.

References

Anders, F., Chiappini, C., Santiago, B. X., et al. 2014, A&A, 564, A115, doi: 10.1051/0004-6361/201323038

Bergsten, G. J., Pascucci, I., Mulders, G. D., Fernandes, R. B., & Koskinen, T. T. 2022, AJ, 164, 190, doi: 10.3847/1538-3881/ac8fea

Borucki, W. J., Koch, D., Basri, G., et al. 2010, Science, 327, 977, doi: 10.1126/science.1185402

Bryson, S., Kunimoto, M., Kopparapu, R. K., et al. 2021, AJ, 161, 36, doi: 10.3847/1538-3881/abc418

Cabral, N., Lagarde, N., Reylé, C., Guilbert-Lepoutre, A., & Robin, A. C. 2019, A&A, 622, A49, doi: 10.1051/0004-6361/201833750

Chabrier, G., Johansen, A., Janson, M., & Rafikov, R. 2014, in Protostars and Planets VI, ed. H. Beuther, R. S. Klessen, C. P. Dullemond, & T. Henning, 619–642, doi: 10.2458/azu_uapress_9780816531240-ch027

Dawson, R. I., & Johnson, J. A. 2018, ARA&A, 56, 175, doi: 10.1146/annurev-astro-081817-051853

Dawson, R. I., & Murray-Clay, R. A. 2013, ApJ, 767, L24, doi: 10.1088/2041-8205/767/2/L24

Deming, D., Knutson, H., Kammer, J., et al. 2015, ApJ, 805, 132, doi: 10.1088/0004-637X/805/2/132

Eilers, A.-C., Hogg, D. W., Rix, H.-W., et al. 2022, ApJ, 928, 23, doi: 10.3847/1538-4357/ac54ad

Fernandes, R. B., Mulders, G. D., Pascucci, I., Mordasini, C., & Emsenhuber, A. 2019, ApJ, 874, 81, doi: 10.3847/1538-4357/ab0300

Fischer, D. A., & Valenti, J. 2005, ApJ, 622, 1102, doi: 10.1086/428383

Fulton, B. J., Petigura, E. A., Howard, A. W., et al. 2017, AJ, 154, 109, doi: 10.3847/1538-3881/aa80eb

Fulton, B. J., Rosenthal, L. J., Hirsch, L. A., et al. 2021, ApJS, 255, 14, doi: 10.3847/1538-4365/abfcc1

Gaudi, B. S. 2012, ARA&A, 50, 411, doi: 10.1146/annurev-astro-081811-125518

Ghezzi, L., Cunha, K., Smith, V. V., et al. 2010, ApJ, 720, 1290, doi: 10.1088/0004-637X/720/2/1290

Hayden, M. R., Bovy, J., Holtzman, J. A., et al. 2015, ApJ, 808, 132, doi: 10.1088/0004-637X/808/2/132
Ida, S., & Lin, D. N. C. 2004, ApJ, 604, 388, doi: 10.1086/381724
Johnson, J. A., Aller, K. M., Howard, A. W., & Crepp, J. R. 2010, PASP, 122, 905, doi: 10.1086/655775
Kunimoto, M., & Matthews, J. M. 2020, AJ, 159, 248, doi: 10.3847/1538-3881/ab88b0
Li, C., & Zhao, G. 2017, ApJ, 850, 25, doi: 10.3847/1538-4357/aa93f4
Li, C., Zhao, G., Zhai, M., & Jia, Y. 2018, ApJ, 860, 53, doi: 10.3847/1538-4357/aac50f
Luque, R., & Pallé, E. 2022, Science, 377, 1211, doi: 10.1126/science.abl7164
Montet, B. T., Yee, J. C., & Penny, M. T. 2017, PASP, 129, 044401, doi: 10.1088/1538-3873/aa57fb
Mordasini, C., Alibert, Y., Klahr, H., & Henning, T. 2012, A&A, 547, A111, doi: 10.1051/0004-6361/201118457
Natta, A., Testi, L., Calvet, N., et al. 2007, in Protostars and Planets V, ed. B. Reipurth, D. Jewitt, & K. Keil, 767, doi: 10.48550/arXiv.astro-ph/0602041
Penny, M. T., Gaudi, B. S., Kerins, E., et al. 2019, ApJS, 241, 3, doi: 10.3847/1538-4365/aafb69
Petigura, E. A., Marcy, G. W., Winn, J. N., et al. 2018, AJ, 155, 89, doi: 10.3847/1538-3881/aaa54c
Pollack, J. B., Hubickyj, O., Bodenheimer, P., et al. 1996, Icarus, 124, 62, doi: 10.1006/icar.1996.0190
Pontoppidan, K. M., Salyk, C., Bergin, E. A., et al. 2014, in Protostars and Planets VI, ed. H. Beuther, R. S. Klessen, C. P. Dullemond, & T. Henning, 363–385, doi: 10.2458/azu_uapress_9780816531240-ch016
Sanders, J. L., & Binney, J. 2015, MNRAS, 449, 3479, doi: 10.1093/mnras/stv578
Surot, F., Valenti, E., Gonzalez, O. A., et al. 2020, A&A, 644, A140, doi: 10.1051/0004-6361/202038346
Wang, J., & Fischer, D. A. 2015, AJ, 149, 14, doi: 10.1088/0004-6256/149/1/14
Wilson, R. F., Cañas, C. I., Majewski, S. R., et al. 2022, AJ, 163, 128, doi: 10.3847/1538-3881/ac3a06
Wilson, R. F., Barclay, T., Powell, B. P., et al. 2023, Submitted, arXiv:2305.16204, doi: 10.48550/arXiv.2305.16204